ENGINEERING TRANSACTIONS • *Engng. Trans.* • **45**, 3–4, 349–362, 1997
Polish Academy of Sciences • Institute of Fundamental Technological Research

NUMERICAL SOLUTION OF THE VISCOUS FLOW PAST A CIRCULAR CYLINDER UNDER THE INFLUENCE OF A MAGNETIC FIELD

M. MORZYŃSKI (POZNAŃ)

E. GÜRGEY and F. THIELE (BERLIN)

The steady laminar incompressible viscous flow over an insulated circular cylinder is investigated. The flow is subjected to an external uniform magnetic field. Besides the familiar Reynolds number, the flow structure also depends on the Hartmann number. A fully implicit finite difference method based on the stream function formulation of the Navier–Stokes equations is used to solve the problem numerically. The magnetic field has a significant influence on the flow, it can delay or even completely cancel the development of the wake and the separation. The flow tends to be more stable since the convection process is suppressed by the magnetic field. Furthermore the drag is increased although the separation is absent.

NOTATIONS

$\mathbf{B}$ magnetic flux density vector,
C_D drag coefficient,
C_{DP} pressure drag coefficient,
C_L lift coefficient,
C_P pressure coefficient,
d diameter of the cylinder,
$\mathbf{E}$ electric field vector,
g_{ij} coefficients of the metric tensor,
$g(\xi,\eta)$ arbitrary two-dimensional function,
Ha Hartmann number $= \sqrt{\mathrm{Re}\, R_m R_h}$,
$\mathbf{J}$ conduction current density vector,
L_W wake length,
N interaction parameter $= \mathrm{Ha}^2/4\mathrm{Re}$,
p pressure,
p_f pressure in front stagnation point,
p_r pressure in rear stagnation point,
Re Reynolds number $= \varrho U_\infty d/\mu$,
R_h magnetic pressure number $= |\mathbf{B}_\infty|^2/U_\infty^2 \varrho \mu_e$,
R_m magnetic Reynolds number $= \sigma U_\infty d \mu_e$,
t time,
$\mathbf{U}_{\mathrm{conv}}$ vector of convection velocity,
U_∞ free stream velocity,
$\mathbf{v}$ velocity vector,
(x,y) Cartesian coordinates,

Greek letters

$\alpha(\xi)$ stretching function in ξ-direction,
$\beta(\eta)$ stretching function in η-direction,
φ angle measured clockwise,
ϱ density of fluid,
μ viscosity of fluid,
μ_e magnetic permeability,
σ electric conductivity of fluid,
ω vorticity,
ω_w wall vorticity,
θ_s wake separation angle,
(ξ, η) curvilinear coordinates,
$\boldsymbol{\psi}$ stream function vector,
ψ scalar stream function,

Subscripts

∞ free stream quantity,
n normal component,
s tangential component,

Operators

∇ nabla operator,
Δ Laplace operator,
$\mathcal{L}$ convection operator.

1. Introduction

In the flow of a conducting fluid such like liquid metal around an obstacle, besides the familiar aerodynamic forces, additional forces are acting on the body if the whole domain is under the influence of the external magnetic field. The Ohm's law of electrodynamics describes the induction of electrical current due to the interaction between the magnetic and velocity fields. The system responds to this induced current with electromagnetic forces acting on the body. Also the external magnetic field experiences small changes. In the present work, the steady liquid metal flow around a circular cylinder is considered. The influence of the flow parameters, the Reynolds number and the Hartmann number, on the near-wake development of the flow is investigated. Although the problem has formerly been attacked by a number of researchers [1, 2], there is still a lack of understanding concerning the physics of the flow over a circular cylinder which could be very helpful for industrial applications [3]. In this work, a very efficient fully implicit finite-difference method based on the stream function formulation of the Navier - Stokes equations [4, 5] is presented to solve the problem numerically.

2. Governing equations

Consideration of the governing equations and the boundary conditions are presented for the unsteady case, although in the present work only the results of steady flows are included. Since the developed solution method incorporates both steady and unsteady flow solutions, this more general case is discussed in the following chapters. The governing equations are the continuity equation, Navier-Stokes equations, and the Maxwell equations which are given in the following non-dimensional form:

$$\nabla \cdot \mathbf{v} = 0, \tag{2.1}$$

$$\frac{D\mathbf{v}}{Dt} = -\nabla p + \frac{1}{\mathrm{Re}} \triangle \mathbf{v} + N(\mathbf{J} \times \mathbf{B}), \tag{2.2}$$

$$\nabla \cdot \mathbf{B} = 0, \qquad \nabla \cdot \mathbf{J} = 0. \tag{2.3}$$

Using the Ohm's law

$$\mathbf{J} = \mathbf{E} + \mathbf{v} \times \mathbf{B} = \frac{1}{R_m}(\nabla \times \mathbf{B}) \tag{2.4}$$

which describes the interaction between the magnetic and the velocity field, the assumption that the electrical current density $\mathbf{J}$ vanishes at infinity leads to:

$$\mathbf{E}_\infty = -\mathbf{v}_\infty \times \mathbf{B}_\infty . \tag{2.5}$$

Equation (2.5) implies that the electric field vector $\mathbf{E}$ becomes zero if the magnetic field acts parallel to the free stream. Besides the Reynolds number Re, two additional independent flow parameters appear in the system of differential equations given in Eqs. (2.1)-(2.4). R_m is the magnetic Reynolds number which determines the perturbation of the external magnetic field due to the interaction with the flow field. N is the so-called interaction parameter which is a measure of the ratio of the electromagnetic to the inertia forces. Frequently another non-dimensional flow parameter is derived to describe the electromagnetic effects, namely the Hartmann number Ha. By taking the rotation of the Navier-Stokes equations (2.2), the pressure term can be eliminated and one obtains the vorticity-transport equations. Introducing the stream function vector $\boldsymbol{\psi}$ which equals the scalar ψ in two-dimensional case as the one and only dependent variable, leads to the stream function equation:

$$\left[\frac{\partial}{\partial t} + (\nabla \times \boldsymbol{\psi}) \cdot \nabla - \frac{1}{\mathrm{Re}} \triangle\right] \triangle \boldsymbol{\psi} = \nabla \times N\left[(((\nabla \times \boldsymbol{\psi}) - \mathbf{v}_\infty) \times \mathbf{B}) \times \mathbf{B}\right]. \tag{2.6}$$

Equation (2.6) is a highly nonlinear, fourth-order partial differential equation, where $\boldsymbol{\psi} = (0, 0, \psi)$ in two spatial dimensions.

3. Boundary conditions

The no-slip and impermeability conditions on the solid body are formulated as the Dirichlet and Neumann boundary conditions in terms of the stream function:

$$\begin{aligned} &\text{No-slip}: && \frac{\partial \psi}{\partial n} = 0, \\ &\text{Impermeability}: && \psi = C. \end{aligned} \tag{3.1}$$

The choice of the constant C appearing in Eq. (3.1) is trivial in case of the circular cylinder flow. Due to the symmetry, the constant is set to zero whereas in case of asymmetric flow its value may strongly deviate from zero. In this case it is calculated iteratively in order to ensure the single-valuedness of pressure thus the conservation of vorticity [6]. At the inflow which is defined as the upstream half of the circular farfield boundary, the flow is assumed to take an asymptotic behaviour which simply implies a potential flow under the influence of the external magnetic field.

For the external flows in the downstream portion of the field boundary, the boundary conditions are not known *a priori*. They are generally a part of the solution since there is no physical boundary. By setting a fictitious downstream boundary, the flow domain is simply cut at a finite distance from the solid body. Any boundary condition which does not take account of the physics would fail to predict the wake development behind the solid body precisely, even if the resulting flow field seems to be correct. One has to impose the boundary conditions which do not force the flow to take a certain shape at the outflow, such like the Dirichlet and Neumann boundary conditions. They simply have to let the physics happen using as few reasonable assumptions as possible.

The flow over bluff bodies like circular cylinders leads to large separated regions and wake structures where the flow quantities are consequently convected downstream. A proper boundary condition should allow these quantities to pass through the boundary. In the present work, the so-called "convective" boundary conditions are applied at the outflow boundary, which are based on the frozen vector field assumption. This implies that there is only the convection process taking place at the outflow boundary. The convection operator

$$\mathcal{L} = \left[\frac{\partial}{\partial t} + \mathbf{U}_{\text{conv}} \cdot \nabla\right] \tag{3.2}$$

can be applied to any physical quantity of interest, which is assumed to be convected with a certain velocity $\mathbf{U}_{\text{conv}}$. The choice of the convection velocity is somehow individual. In the present work, the convection of vorticity

$$\left[\frac{\partial}{\partial t} + (\nabla \times \boldsymbol{\psi}) \cdot \nabla\right] \triangle \boldsymbol{\psi} = 0 \tag{3.3}$$

is assumed to take place with the local velocity $(\nabla \times \boldsymbol{\psi})$. Obviously Eq. (3.3) is nothing but the stream function equation (2.6) without the viscous and magnetic terms implying that the flow is convected as a frozen vector field. On the other hand, the normal component of the impulse is allowed to be convected with the free stream velocity $\mathbf{U}_\infty$ so that the pressure gradient at the outflow boundary is not forced to vanish

$$\left[\frac{\partial}{\partial t} + \mathbf{U}_\infty \cdot \nabla\right] (\nabla \times \boldsymbol{\psi})_n = 0. \tag{3.4}$$

Indeed most of the wake structures behind the bluff bodies are of Oseen-Hamel type having non-zero pressure gradients which is also confirmed by experimental investigations [7]. The convection operator (3.2) can similarly be applied to the other flow quantities like the stream function itself

$$\left[\frac{\partial}{\partial t} + \mathbf{U}_\infty \cdot \nabla\right] \boldsymbol{\psi} = 0 \tag{3.5}$$

or to the tangential component of the impulse $(\nabla \times \boldsymbol{\psi})_s$. It is noteworthy to mention that the convection of the stream function (3.5) as the outflow boundary condition – although working excellent – is a numerical boundary condition rather than physical since the stream function is not a physical quantity. In the present study, the Eqs. (3.3) – (3.4) are applied as outflow boundary conditions.

4. Numerical procedure

In the stream function equation (2.6), the evolution of the flow in time is given by the local time derivative of $\triangle\boldsymbol{\psi}$ which is discretised by using an implicit Euler approximation. The stream function equation is linearized using the Newton's method.

The spatial discretisation is performed via finite difference formulae generated by the Lagrangian polynomials such that a 13-point finite difference molecule is required to achieve a second order accuracy for the fourth-order derivatives in the viscous term. The convective term is discretised with a fourth-order accuracy which allows accurate computations at moderate to high Reynolds numbers, without any need of imposing additional dissipative terms or upwinding.

The efficiency of the method is significantly improved by introducing Chord-iterations where only the right-hand-side vector is updated. After every Newton iteration, the LU decomposed matrix is stored for the next three Chord-iterations. In general, only one Newton iteration and three Chord-iterations are enough to achieve a residuum of the order of 10^{-6}. For complex flow problems like high

Reynolds number flows or flows which possess high unsteadiness, an additional Newton iteration may be required.

Once the stream function equation is solved, the components of the pressure gradient can be calculated explicitly from the Navier-Stokes equations in primitive variables since all the other terms can be expressed by the stream function. The pressure field is then obtained by the line integration of the pressure gradient where the result is independent of the integration path.

The computational grid is an orthogonal O-grid generated by a conformal mapping procedure [4] which leads, in case of a circular geometry, to the well known exponential-polar coordinates. The analytical calculation of the metric quantities of the transformation to the equidistant rectangular domain avoids possible numerical errors since the derivatives of these quantities up to the third order appear in the stream function equation (2.6). In order to simplify the stream function equation, a further specialization of the metric coefficients is introduced in the following form

$$g_{11} = \alpha^2(\xi)g(\xi,\eta), \qquad g_{22} = \beta^2(\eta)g(\xi,\eta), \tag{4.1}$$

which is particularly valid for any conformal mapping procedure.

5. Results

As mentioned before, the present work deals with the steady MHD-flow over an insulated circular cylinder. Special attention is paid to the computation of the aerodynamic coefficients in order to predict the influence of the magnetic field on the flow structure.

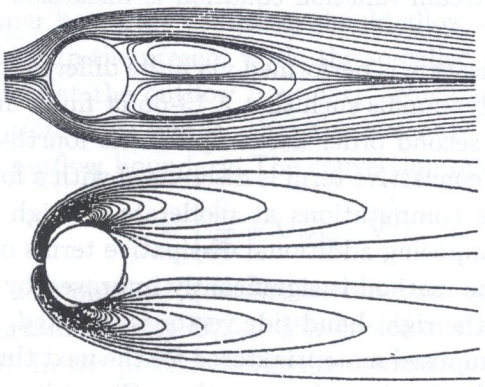

FIG. 1. Viscous flow over a circular cylinder. Re = 40, $N = 0$. a) Streamlines. b) Vorticity isolines.

In order to validate the numerical procedure, a test study is conducted for the flow around a circular cylinder without magnetic field. This case has been investigated formerly by numerous researchers [8–12]. In Fig. 1 the isolines of the stream-function and vorticity are shown for Re = 40. A symmetric pair of vortices is developed giving rise to symmetric separation bubbles behind the cylinder. Due to the symmetry of the flow, no lift is produced. The comparison of the computed drag coefficient and the length of the separation bubble with experimental and numerical results shows an excellent agreement (Table 1).

Table 1. Flow characteristics for Re = 40 without a magnetic field.

Author	θ_s	L_w/d	C_D	C_{DP}/C_D	p_f	p_r
Grove *et al.*, (exp) [8]	–	–	–	–	1.175	−0.525
Coutanceau & Bouard (exp) [9]	–	2.63	–	–	–	–
Collins & Dennis, 1973 (num)	53.6	2.65	1.560	0.654	1.160	−0.530
Fornbeg, (num) [1]	53.8	2.74	1.498	–	1.140	−0.460
Franke & Schönung, (num) [12]	53.8	2.86	1.520	0.655	1.160	−0.490
Present work	53.8	2.69	1.571	0.656	1.152	−0.515

Imposing the magnetic field acting parallel to the free stream, changes the flow field in such a way that the separation bubbles become smaller or even disappear (Fig. 2). For Re = 40 no separation occurs if N exceeds the value 0.3. Streamline

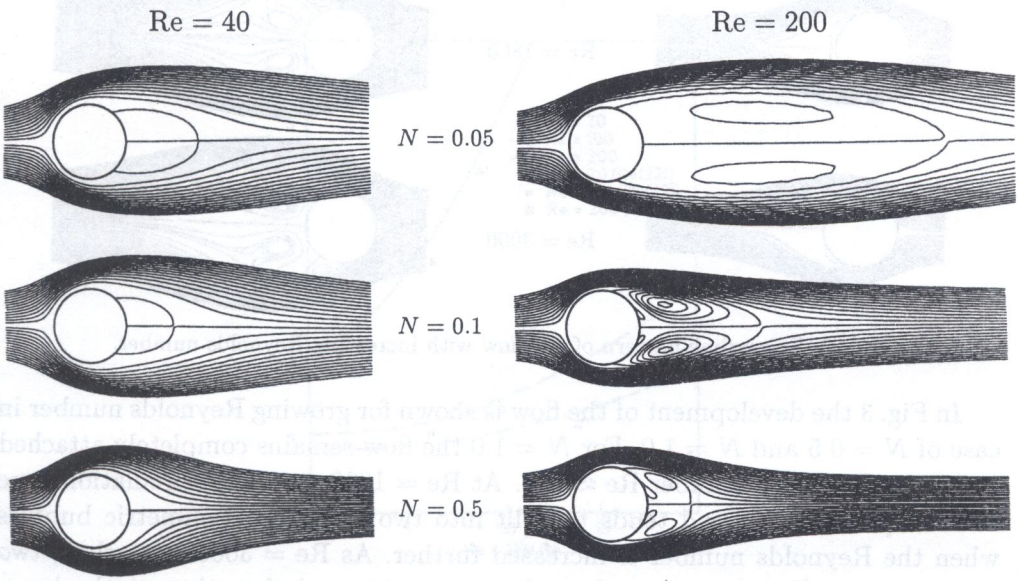

FIG. 2. Near-wake structure.

patterns for Re = 200 and $N \geq 0.1$ indicate two additional symmetric vortices with their centers lying in the immediate neighbourhood of the cylinder wall. The magnetic field obviously suppresses the convection and diffusion processes and stabilizes the flow. Consequently the periodic vortex shedding which appears at Reynolds numbers higher than a critical value slightly above 40 is delayed.

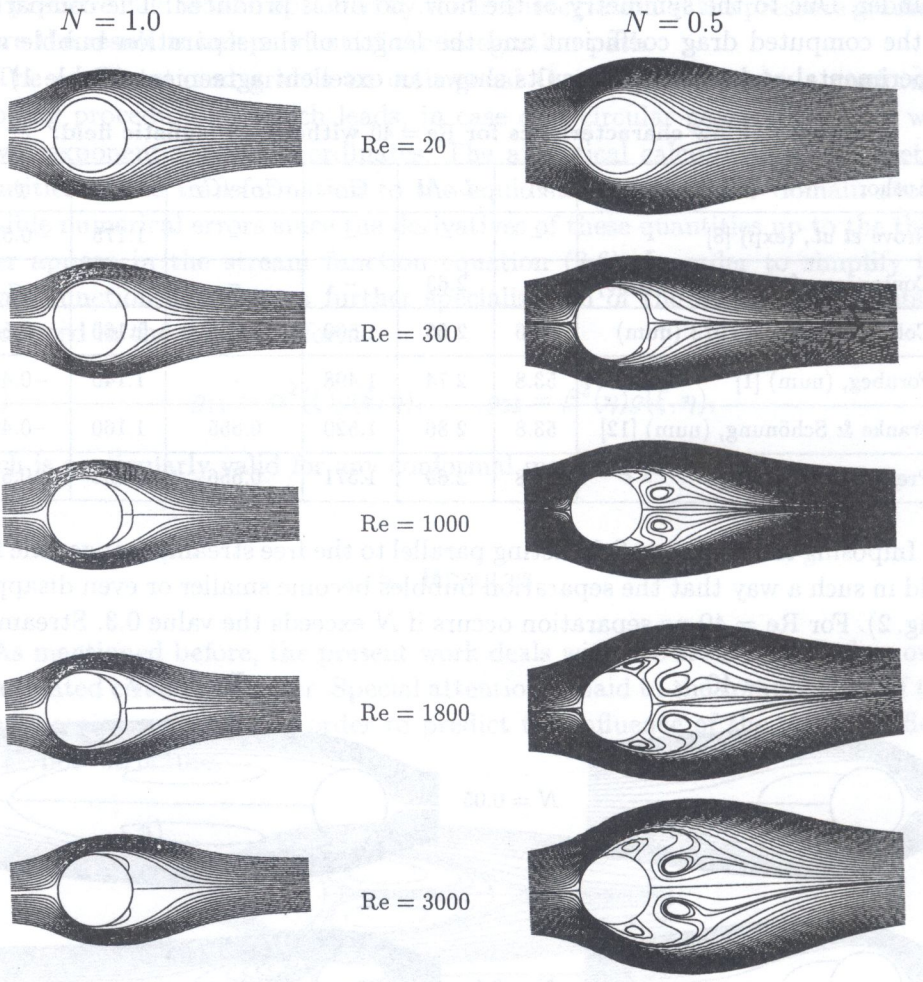

FIG. 3. Streamline pattern of the flow with increasing Reynolds number.

In Fig. 3 the development of the flow is shown for growing Reynolds number in case of $N = 0.5$ and $N = 1.0$. For $N = 1.0$ the flow remains completely attached up to the Reynolds number Re ≈ 800. At Re = 1000 a small recirculation zone is already developed and tends to split into two separated symmetric bubbles when the Reynolds number is increased further. As Re = 3000 is reached, two symmetric bubbles appear: one at the upper side and the other at the lower

side of the cylinder. Both separation points are placed more upstream than in case of vanishing magnetic field. As the Reynolds number is growing further, the bubbles seem to become smaller again and they completely disappear at Re $\approx$ 5000. This peculiar behaviour is caused probably by the fact that at those Reynolds numbers where separation occurs, still the effect of diffusion exists. For higher N, the magnetic field effects get stronger and no separation is observed at all.

Both the convection and diffusion are cancelled by the magnetic field which absolutely dominates the flow field. For $N = 0.5$ the increment of the Reynolds number causes interesting flow structure in the near-wake region. The wake is expanded in vertical direction and contains more than only two vortex pairs. Streamline patterns for Re = 300 are similar to that observed for $N = 1.0$ at Re $\approx$ 3000. As the Reynolds number is increased further, the separation points on both sides of the cylinder travel upstream and additional vortices appear in the near-wake region. Two pairs of bubbles are identified as primary vortices. One pair is attached to the wall and the other is detached. There are even more smaller vortex formations, especially when the Reynolds number is increased further. In the case of a magnetic field acting parallel to the free stream ($\varphi = 0$), the flow remains symmetric, hence no lift is produced whereas the drag is increased surprisingly. The primary contribution to the drag comes from the pressure distribution on the surface of the circular cylinder. Figure 4 shows the variation of the total drag coefficient C_D with the Hartmann number Ha. As seen in Table 2, the ratio of the pressure drag C_{DP} to the total drag increases for

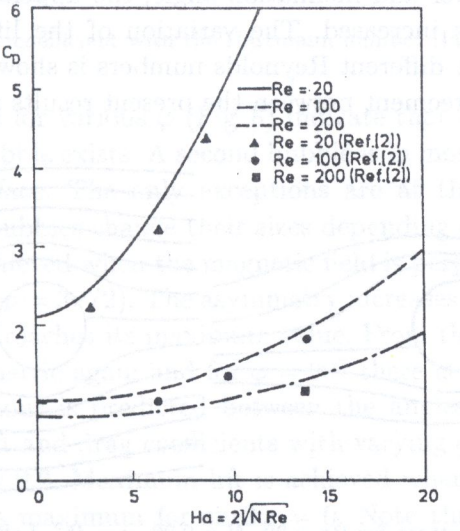

FIG. 4. Variation of the drag with the Hartmann number Ha.

Table 2. Variation of the flow characteristics with N.

N	L_w/d	C_D	C_{DP}/C_D	Front stag. press.	Rear stag. press.
0.05	1.610	1.897	0.682	1.158	−0.794
0.1	1.313	2.113	0.690	1.161	−1.007
0.2	0.857	2.481	0.703	1.169	−1.383
0.5	–	3.351	0.729	1.181	−2.295
1.0	–	4.534	0.757	1.200	−3.537
3.0	–	8.296	0.808	1.216	−7.804
5.0	–	11.412	0.832	0.774	−11.903

growing N clearly indicating that the suction region behind the cylinder becomes stronger and determines the aerodynamic behaviour. For moderate values of N the front stagnation pressure does not vary significantly with increasing N. The symmetry of the flow deteriorates if the magnetic field is inclined to the free stream by the angle of φ which is measured clockwise from the x-axis. In this case lift is produced due to the non-symmetric pressure and vorticity distributions. The streamline plots are shown in Figs. 5 and 6 in comparison with those of Ref. [2]. For $\mathrm{Re} = 20$, $\mathrm{Ha} = 8.9$, $\varphi = 45°$ the flow does not separate but becomes non-symmetric. Two almost stable separation bubbles with slightly smaller upper one are observed behind the cylinder for $\mathrm{Re} = 100$, $\mathrm{Ha} = 14.1$, $\varphi = 9°$. For the same Reynolds number and inclination angle, the upper bubble vanishes if the Hartmann number is increased. The variation of the lift coefficient with the Hartmann number at different Reynolds numbers is shown in Fig. 7. There is a good quantitative agreement between the present results and those of Ref. [2].

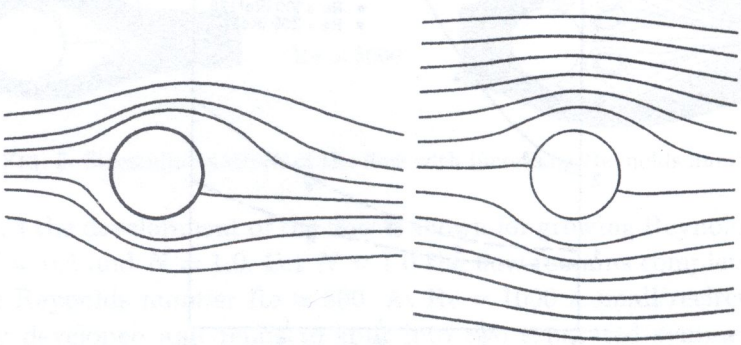

FIG. 5. Streamline pattern for $\mathrm{Re} = 20$, $N = 0.99$, $\varphi = 45°$. Left: Present work, right: MOCHIMARU, 1992 [2].

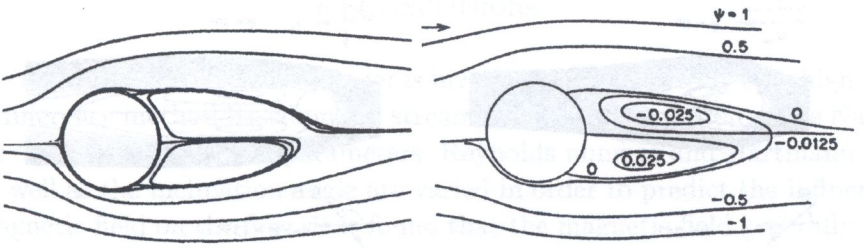

FIG. 6. Streamline pattern at Re = 100, $N = 0.099$, $\varphi = 9°$. Left: Present work, right: Mochimaru, 1992 [2].

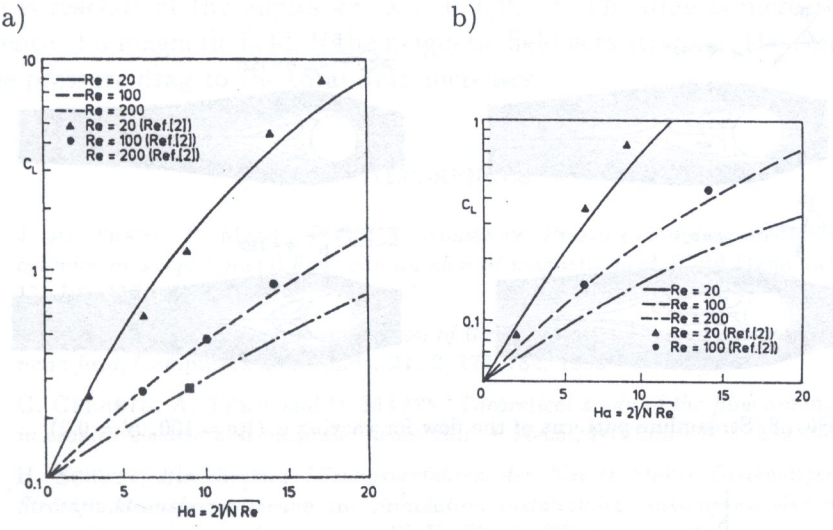

FIG. 7. Variation of the lift coefficient with the Hartmann number Ha; a) $\varphi = 9°$, b) $\varphi = 45°$.

Streamline patterns for various φ (Fig. 8) indicate that for all φ at least one standing separation bubble exists. A second bubble is in most cases disconnected from the cylinder surface. The only exceptions are at the angles $\varphi = k\pi/2$ $(k = 0, 1, 2, ...)$. Both bubbles change their sizes depending on φ. The maximum separation length is achieved when the magnetic field is perpendicular to the free stream (i.e $\varphi = \pi/2$ or $\varphi = 3\pi/2$). The asymmetry increases with growing φ until $\varphi = 45°$ where the lift reaches its maximum value. From this angle on, the flow tends to become symmetric again and for $\varphi = 90°$ there is already a symmetric flow. A similar behaviour is predicted between the angles 90° and 180°. The developments of the lift and drag coefficients with varying φ are shown in Fig. 9 for Re = 100 and $N = 0.2$. Maximum lift is achieved when $\cos 2\varphi = 0$ whereas absolute drag becomes maximum for $\sin 2\varphi = 0$. Note that the drag becomes nearly zero for $\varphi = 90°$ and changes the sign for $90° < \varphi < 180°$.

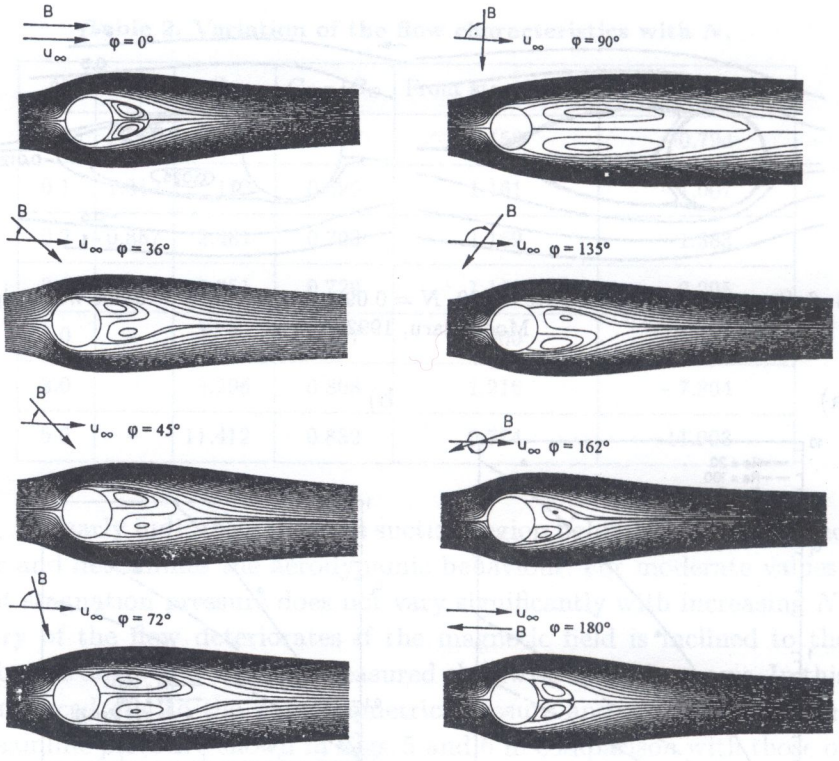

FIG. 8. Streamline patterns of the flow for varying φ (Re = 100, $N = 0.2$).

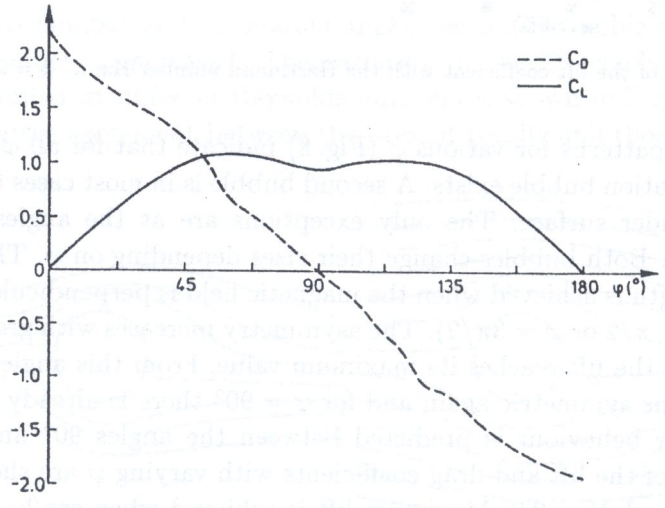

FIG. 9. Development of the lift and drag coefficients for varying φ.

6. Conclusions

The flow around a circular cylinder is investigated numerically by a high-order finite difference method based on the stream-function formulation of the Navier - Stokes equations. Both flow parameters, Reynolds number and Hartmann number as well as the inclination angle are varied in order to predict the influence of the magnetic field on the flow. It is found that the magnetic field generally tends to suppress the near, wake development and stabilize the flow. If $\sin 2\varphi = 0$, the flow remains fully symmetric, hence no lift is produced. Otherwise the lift produced is nearly proportional to the Hartmann number and its maximum absolute value is reached at the angles $k\pi$ $(k = 0, 1, 2, ...)$. The drag is increased by the existence of a magnetic field. If the magnetic field gets stronger, the contribution of the pressure drag to the total drag increases.

References

1. J. Josserand, P. Marty P and A. Alemany, *Pressure and drag measurements on a cylinder in a liquid metal flow with an aligned magnetic field*, Fluid Dynamics Research, **11**, 107–117, 1993.
2. Y. Mochimaru, *Numerical simulation of the flow past a circular cylinder under a magnetic field*, Computers and Fluids, **21**, 2, 177–184, 1992.
3. G. Gerbeth, A. Thess and P. Marty, *Theoretical study of the flow around a cylinder in crossed electric and magnetic fields*, Eur. J. Mech., B/Fluids, **9**, 3, 239–257, 1990.
4. H. Schütz, *Ein direktes Lösungsverfahren der Navier–Stokes Gleichungen in reiner Strömfunktionsformulierung zur Simulation instationärer inkompressibler Strömungen in zweidimensionalen Geometrien*, Ph.D. Thesis, TU-Berlin 1990.
5. M. Morzyński and F. Thiele, *Numerical stability analysis of the flow about a cylinder*, Z. Angew. Math. Mech., 71, **5**, T424-428, 1991.
6. E. Gürgey and F. Thiele, *Numerical simulation of the viscous flow over an oscillating airfoil, experimental and numerical flow visualisation*, ASME FED – Vol. 128, B. Khalighi *et al.* [Eds.], presented at the Winter Annual Meeting of ASME, Atlanta, Georgia, December 1-6, 1991.
7. A. Timme, *Über die Geschwindigkeitsverteilung in Wirbeln*, Ing. Arch., **25**, 205–225, 1957.
8. A.S. Grove, F.H. Shair, E.E. Petersen and A. Acrivos, *An experimental investigation of the steady separated flow past a circular cylinder. Part 1*, J. Fluid Mech., **19**, 60–79, 1964.
9. M. Coutanceau and R. Bouard, *Experimental determination of the main features of the viscous flow in the wake of a circular cylinder in uniform translation. Part 1. Steady flow*, J. Fluid Mech., **79**, 231–256, 1977.
10. W.M. Collins and S.C.R. Dennis, *Flow past an impulsively started circular cylinder*, J. Fluid Mech., **60**, 105–127, 1973.

11. B. FORNBERG, *A numerical study of steady viscous flow past a circular cylinder*, J. Fluid Mech., **98**, 819–855, 1980.

12. R. FRANKE and B. SCHÖNUNG, *Die numerische Simulation der laminaren Wirbelablösung an Zylindern mit quadratischen oder kreisförmigen Querschnitten*, SFB 210/T/39, 1988.

POZNAŃ UNIVERSITY OF TECHNOLOGY, POZNAŃ, POLAND

e-mail: morzynski@stanton.bmd.put.poznan.pl

and

HERMANN-FÖTTINGER-INSTITUT FÜR STRÖMUNGSMECHANIK, TU-BERLIN, GERMANY

e-mail: thiele@pi.tu-berlin.de

Received January 17, 1997; new version June 16, 1997.